Hindawi Publishing Corporation
Mathematical Problems in Engineering
Volume 2016, Article ID 8704134, 8 pages
http://dx.doi.org/10.1155/2016/8704134

Research Article

In Situ Measurement of Wind-Induced Pulse Response of Sound Barrier Based on High-Speed Imaging Technology

Chunli Zhu,[1,2] Jie Guo,[2] Dashan Zhang,[2] Yuan Shen,[1] and Dongcai Liu[1]

[1]*School of Electronic and Information Engineering, Hefei Normal University, Hefei 230601, China*
[2]*Department of Precise Machine and Precise Instrument, University of Science and Technology of China, Hefei 230027, China*

Correspondence should be addressed to Dongcai Liu; liudc_hf@foxmail.com

Received 5 April 2016; Accepted 10 August 2016

Academic Editor: Filippo Ubertini

The lifetime of the sound barrier is threatened by high-speed train-induced impulsive wind pressure as it passes by. The vibration response of the sound barrier during the process of train passing is difficult to be measured using conventional measurement methods because of the inconvenience of the installation of markers on the sound barrier. In this paper, the high-speed camera is used to record the whole process of the train passing by the sound barrier. Then, a displacement extraction algorithm based on the theory of Taylor expansion is proposed to obtain the vibration response curve. Compared with the result simulated by using the finite element method, the video extraction result shows the same head wave and tail wave phenomenon, demonstrating that the vibration measurement by using the high-speed imaging technology is an effective measuring way. It can achieve noncontact and remote vibration measurement and has important practical value.

1. Introduction

A sound barrier also called a noise barrier, sound berm, or acoustical barrier is an exterior structure designed to absorb and reduce generated impulsive noise and vibration energy, protecting inhabitants of sensitive land use areas from noise pollution. Sound barriers have been the most effective method of mitigating roadway, railway, and industrial noise sources. With the rising speed of the train, the train can run at a speed up to 250 km/h or faster. With such a high speed, very strong airflow interaction occurs between sound barriers and the train as it passes by. Due to severe compression and expansion of air, strong impulsive air pressure is generated. Under the impulsive pressure, the sound barrier is pulled and pushed repeatedly, eventually leading to fatigue damage of the sound barrier structure. In 2003, the sound barrier erected along the railway between Frankfurt and Cologne of Germany was destroyed under the influence of the impulsive pressure. The reconstruction and maintenance cost amazingly amounted to 30 million euros [1]. Due to the high cost of design, construction, and maintenance of sound barrier, besides ensuring good noise mitigation performance, the sound barrier should also have dynamic mechanical properties to ensure sufficient structural safety. Nowadays, this has become an important topic in the study of sound barrier design.

To explore the influence of the process of train passing on the sound barrier, numerous studies about impulsive wind pressure have been conducted [2–7]. To obtain the time histories of pressure and vehicle aerodynamics, Hermanns et al. applied various implementations of the direct boundary element method (BEM) to solve the Laplace equation, which governs the flow field around the power car of high-speed trains in an approximate manner [2]. Jiao et al. analyzed the influences of the type and speed of trains and the length and height of the noise barrier structures on the dynamic response characteristics of noise barrier structures numerically by using ANSYS software [3]. Zhao et al. obtained the air turbulent force curve by simulating the whole process of train passing using the fluid calculation software CFX [4, 5].

Previous studies about the sound barrier have achieved significant achievements, letting us have a good understanding of the vibration response characteristics of the sound barrier. However, these studies were mainly focused on

simulation analysis of the influence of high-speed trains on the sound barrier by using ANSYS or CFX software. Experimental verification and vibration measurements on real sound barrier structure are rare. One reason is that it is difficult to construct the passing process of high-speed trains and measure the vibration of sound barrier in laboratory conditions. The other reason is that, in conventional vibration measurements, marks, such as acceleration meter probe, should be installed on the detected object. Sound barriers are usually erected along the railway or viaduct, which makes it difficult to install marks on the sound barrier, causing great inconvenience to on-site vibration measurement.

With the development of image processing technology, vibration measurement based on visual has attracted people's attention. It has the advantages of noncontact, remote measurement and no additional mass and does not affect the dynamic characteristics of the detected object [8–12]. Lee and Shinozuka proposed the vision-based system which remotely measures dynamic displacement of bridges in real time using digital image processing techniques [10, 11]. Yang et al. introduced the concept of dynamics-based visual inspection with High-Frame-Rate (HFR) video analysis as a novel nondestructive active sensing method for verifying dynamic properties of a vibrating object [12]. Park et al. realized 3D displacement measurement model for health monitoring of structures using a motion capture system [13]. In view of the above studies, in this paper, firstly the response of sound barrier subjected to train-induced impulsive wind pressure is simulated by using the finite element method. Then the high-speed imaging is used to on-site record the vibration of the sound barrier during the whole process of train passing. In order to achieve the vibration and modal characteristics of the sound barrier, unlike conventional image processing method, a displacement extraction algorithm based on the theory of Taylor expansion is applied to achieve visual tracking of rigid moving objects. This displacement extraction algorithm is fast and has high efficiency. And, in the measurement, vibration displacement can be extracted without installation of marks on the detected object.

2. Simulation of the Vibration Response of the Sound Barrier

Before in situ measurement, the response of the sound barrier subjected to train-induced impulsive wind pressure is simulated by using the finite element method. In our country, there are two types of sound barriers along the high-speed railway, that is, plug-in sound barrier and integral sound barrier. And plug-in sound barrier is the main type. The model of plug-in sound barrier is shown in Figure 1. One sound barrier unit comprises multiblock absorption cell plates and two vertical steel columns.

The dimensions and connection of the plug-in sound barrier are shown in Figure 2. The sound barrier with a full height of 2150 mm is fixed on the viaduct using steel columns with steel type of 175 × 175 H. The distance between steel columns is 2000 mm. Five sound absorption plates are inserted between two adjacent steel columns. The width and thickness of the sound absorption plate are 430 mm and 140 mm. The sound absorption plate comprises three layers: the layer facing the train is cold-formed steel plate with holes; the middle layer is porous sound absorption materials; and the layer facing away from the train is cold-formed steel plate without holes. Sound absorption plates can reduce multiple reflection noise between the high-speed train and the sound barrier.

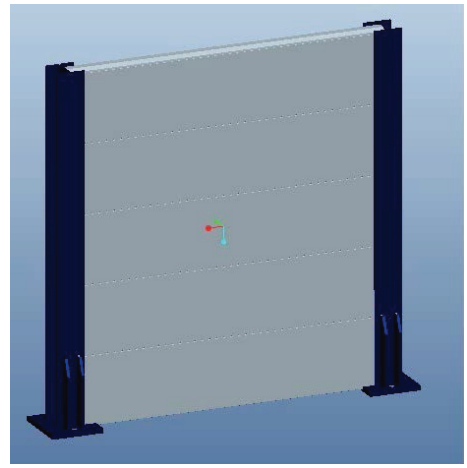

Figure 1: Plug-in sound barrier.

According to actual condition, the model of nine plug-in sound barriers and one expansion joint is simulated using the finite element method. The first 15 natural frequencies of the sound barrier are simulated using the Pro/E Mechanic. The natural frequencies can be roughly divided into three categories. The first category contains first 9 natural frequencies, which are very close and concentrated in the range 10.195~11.283 Hz. The first 9 modes are the first-order vibration of the sound absorption plate. The 10th-order frequency of 21.039 Hz represents the vibration at the expansion joints. The third category contains the 11th- and higher order frequencies, which are about 40 Hz. The 12~15th-order modes are secondary vibration of the sound absorption plate.

Factors causing sound barrier vibration mainly include its own weight, ground vibration, wind, and impulsive wind pressure incited by train passing. When the train passes by the sound barrier with a speed up to 250 km/h or faster, very strong airflow interaction will be generated between the sound barrier and the train, inducing a series of aerodynamic effects and yielding strong transient impulsive pressure. During the process of train passing, this transient impulsive pressure is much greater than other loads. And the faster the train is, the greater the impulsive wind pressure is. According to Zhao et al.'s study [4], the fitted impulsive air pressure curve is used as the structural excitation load when the train passes by, as shown in Figure 3.

The vibration response curve of sound barrier subjected to train-induced impulsive air pressure simulated using the finite element method is shown in Figure 4. One obvious feature of the vibration curve is that it has significant head wave and tail wave phenomenon. When the head of the train reaches the sound barrier, great positive and negative wind

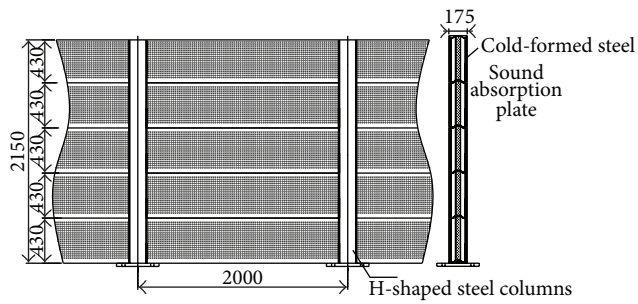

Figure 2: Dimensions of plug-in sound barrier.

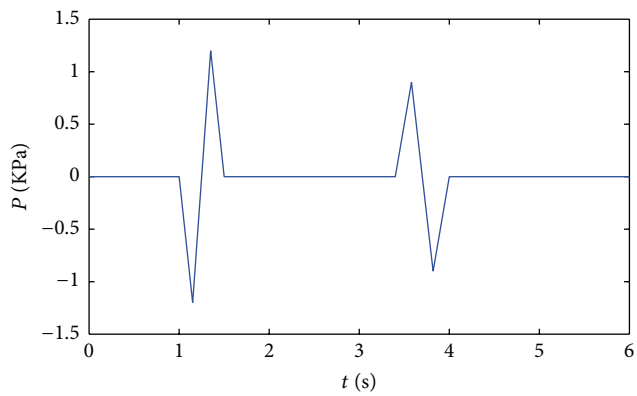

Figure 3: Impulsive air pressure curve.

pressure will be incited to intrude the sound barrier, resulting in head wave response. When the rear of the train leaves the sound barrier, tail wave response with a lower peak value occurs.

3. On-Site Measurement of Sound Barrier Vibration

In situ measurement experiment is conducted under the viaduct of Kunshan segment along the Shanghai-Hefei high-speed railway, shown in Figure 5. Figure 5(a) shows the plug-in sound barrier structure. The shooting target is at the entry position where it has the maximum wind pressure as train passes by, denoted as red box. Figure 5(b) shows the high-speed camera (Nikon VR 70–200 mm) used in our experiment, which has a shooting distance further than 50 m. The high-speed camera is placed below the viaduct. The recorded vibration is the projection of the real vibration, but their waveform and the spectrum are consistent. When the train arrives, the high-speed camera controlled by PC software starts to record the sound barrier vibration during the whole process of train passing. The frame rate and the frame size of the high-speed camera are 230 frames per second and 1880 × 658 pixels. Figure 5(c) gives one frame of sound barrier vibration. It can be seen that the gap between two sound absorption plates becomes uneven due to the influence of train-induced impulsive wind pressure.

It can be seen from the video of the sound barrier vibration that the train reaches the sound barrier at 0.82 s. At this time, the sound barrier is pushed inward obviously by the wind pressure. After that, the sound barrier undergoes continuous rigid oscillation due to the air interaction between the train and the sound barrier. Figure 6 shows 6 frames of sound barrier when it has great vibrations. The vibration is within 10 pixels. It is so small relative to the entire frame that it is very difficult to identify the vibration from the static image by eyes. In the following, image processing algorithm based on Taylor expansion is applied to extract the vibration response of the sound barrier.

4. Sound Barrier Vibration Extraction Algorithm

Feature identification and tracking of the target are operated by means of binarization, edge detection, and opening and closing operation in conventional image processing. For these methods, multiple thresholds are needed; algorithms are time-consuming and inefficient; predesigned special markers are required to be installed on the tracking target. In this section, the displacement automation extraction algorithm based on Taylor expansion is proposed to estimate the rigid vibration of the sound barrier.

The projection of the rigid vibration on the camera performs as overall shift of the sound barrier. Therefore, the vibration response extraction actually is to calculate displacements between every two adjacent images. The response curve over the whole process can then be achieved by accumulating these calculated displacements.

The image analysis model is described as follows. In the kth frame image, the subimage $T(x, y)$ that contains overall motion information is selected as the reference image, as shown in Figure 7. According to the spatial smoothness assumption, from $T(x, y)$ to the next subimage $T'(x, y)$, all pixels in $T(x, y)$ maintain the same displacement $p = (u, v)^T$. The extraction of displacement vector can be realized via image alignment. Align $T'(x, y)$ and the reference image $T(x, y)$ and then the displacement vector p can be extracted in the $(k + 1)$th frame image.

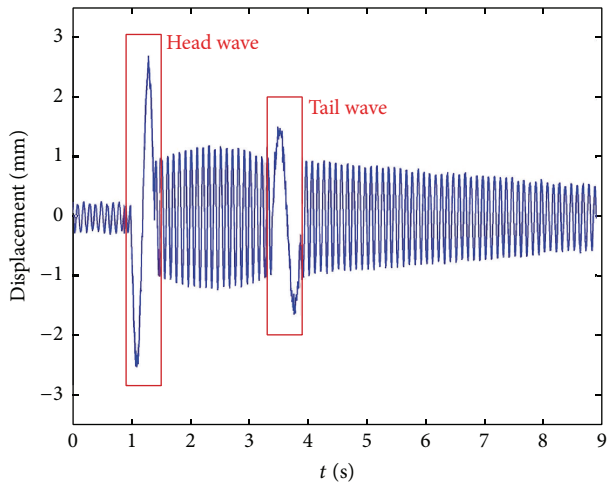

Figure 4: Simulation response of sound barrier subjected to train-induced impulsive air pressure.

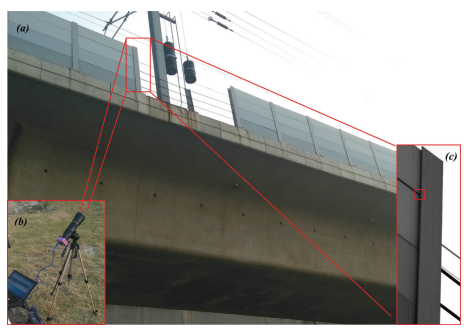

Figure 5: In situ measurement of sound barrier.

In the $(k+1)$th frame image, the subimage that has the same position with $T(x, y)$ is denoted as $I(x, y)$. According to constant brightness and small displacement assumptions, there is

$$I(x, y) = T(x-u, y-v). \tag{1}$$

Operate first-order Taylor expansion. Since the displacement u and v are very small, high order terms can be omitted. Then $I(x, y)$ can be written as

$$I(x, y) = T(x-u, y-v) \approx T(x, y) - uT_x - vT_y \tag{2}$$

and transformed as

$$T(x, y) - I(x, y) = \begin{bmatrix} T_x & T_y \end{bmatrix} \begin{bmatrix} u \\ v \end{bmatrix}, \tag{3}$$

where T_x and T_y are partial derivatives of $T(x, y)$ in the x and y directions.

Because all pixels in $T(x, y)$ move in the same manner, function (3) is effective for all pixels $(x_i, y_i) \in T$, $i \in [1, n]$ (n is the total pixel number of T). Therefore,

$$\begin{bmatrix} T(x_1, y_1) - I(x_1, y_1) \\ T(x_2, y_2) - I(x_2, y_2) \\ \vdots \\ T(x_n, y_n) - I(x_n, y_n) \end{bmatrix} = \begin{bmatrix} T_x(x_1, y_1) & T_y(x_1, y_1) \\ T_x(x_2, y_2) & T_y(x_2, y_2) \\ \vdots & \vdots \\ T_x(x_n, y_n) & T_y(x_n, y_n) \end{bmatrix} \begin{bmatrix} u \\ v \end{bmatrix}. \tag{4}$$

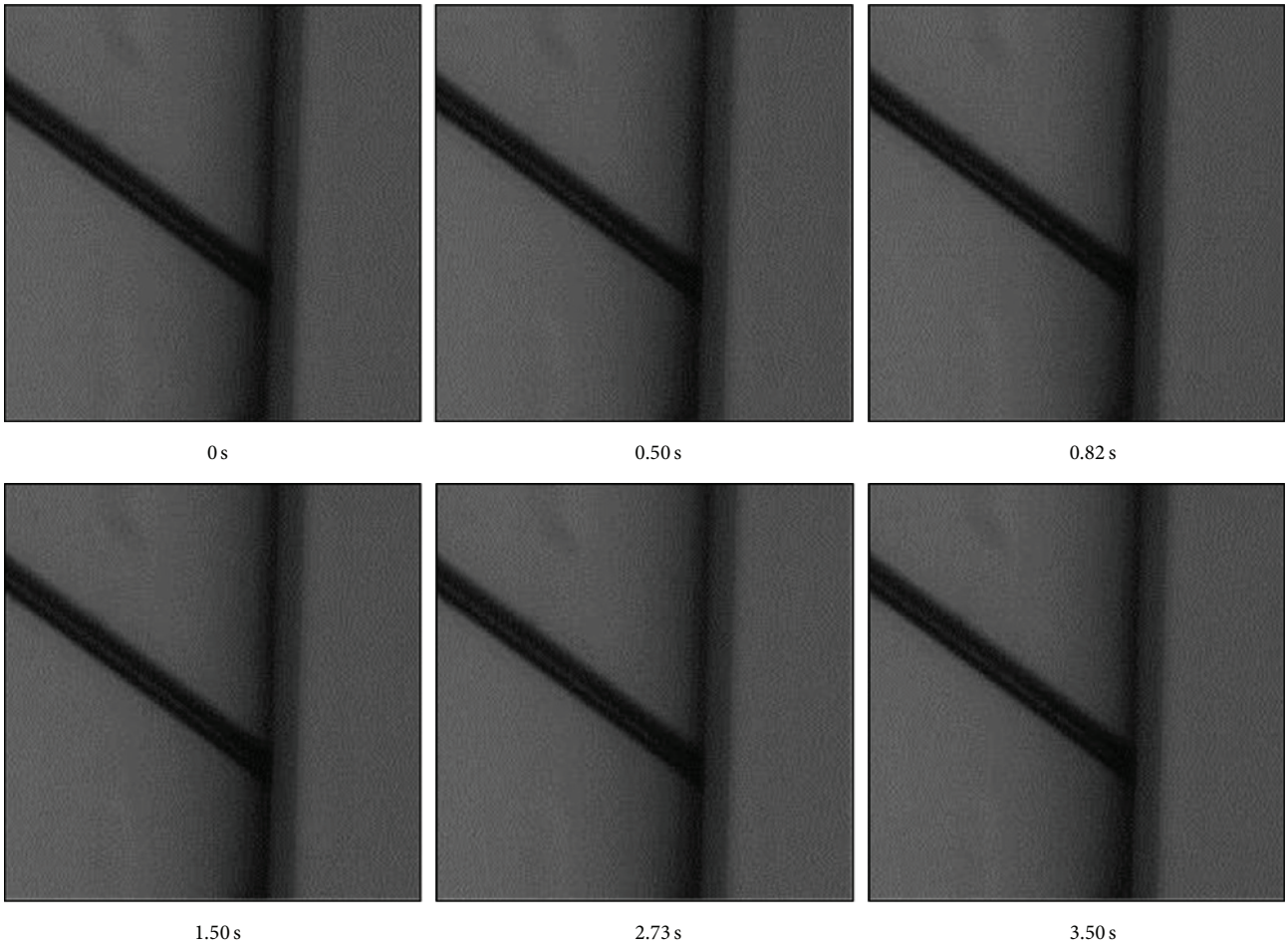

Figure 6: Vibration images of sound barrier.

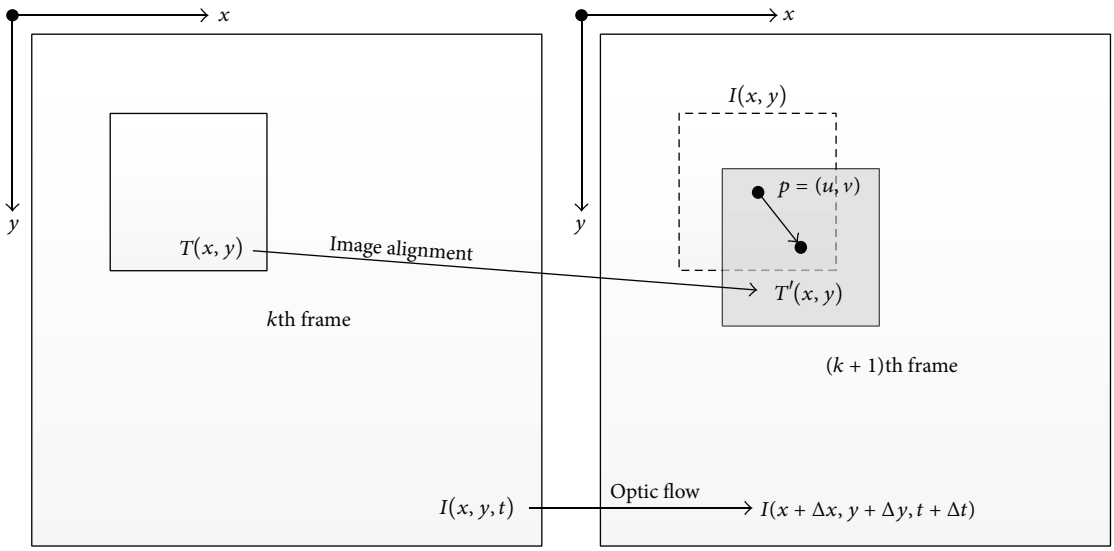

Figure 7: Illustration of displacement extraction.

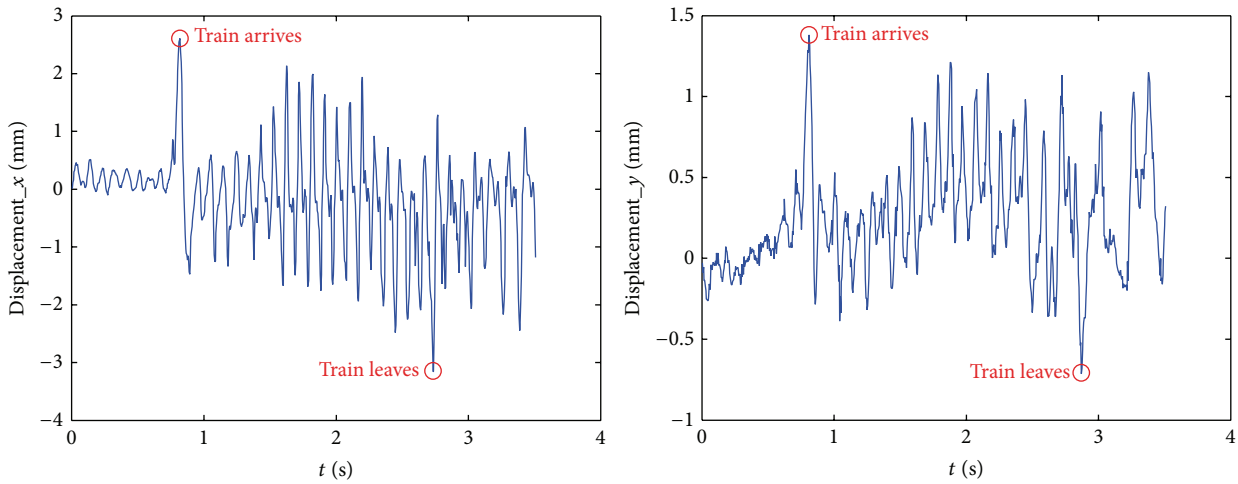

Figure 8: Vibration response curve of sound barrier.

Denote

$$\Delta T = \begin{bmatrix} T(x_1, y_1) - I(x_1, y_1) \\ T(x_2, y_2) - I(x_2, y_2) \\ \vdots \\ T(x_n, y_n) - I(x_n, y_n) \end{bmatrix},$$
$$\nabla T = \begin{bmatrix} T_x(x_1, y_1) & T_y(x_1, y_1) \\ T_x(x_2, y_2) & T_y(x_2, y_2) \\ \vdots & \vdots \\ T_x(x_n, y_n) & T_y(x_n, y_n) \end{bmatrix}. \quad (5)$$

Then, according to the generalized least squares, when $\nabla T^T \cdot \nabla T$ is reversible, there is

$$p_1 = \left[\nabla T^T \cdot \nabla T\right]^{-1} \cdot \nabla T^T \cdot \Delta T. \quad (6)$$

According to the above equations, displacement vector p can then be estimated.

The algorithmic process is summarized as follows:

(1) Select one region $T(x, y)$ that contains overall motion information as the reference image. Intercept the same position $I(x, y)$ in the next frame image.

(2) Use the central difference to calculate partial derivatives of $T(x, y)$ in the x and y directions.

(3) Calculate the difference matrix ΔT and gradient matrix ∇T according to function (5).

(4) Calculate the offset p_i according to function (6).

(5) Update $T(x, y)$ as $T(x\text{-round}(u_i), y\text{-round}(v_i))$ using the calculated p_i. Repeat steps (1) to (4) until the absolute values of u_i and v_i are less than 0.5.

The displacement response curve of rigid vibration can be obtained by applying the above algorithm on the whole video frames. This displacement extraction algorithm is based on the template tracking algorithm. Compared with feature-based conventional image processing, this algorithm has the following characteristics: target tracking is implemented by identifying the boundary or veins of the template so that there is no need to install special markers on the tracking target; threshold selection is also not needed as there is no need of feature extraction operation; this algorithm needs fewer adjustable parameters and is more automated; it has subpixel accuracy and no additional precision optimization algorithm is needed.

This algorithm is different from optical flow method which is also based on Taylor expansion. In optical flow method [14, 15], the velocities and directions of all pixels, that is, the optical flow field, are estimated by using the variation of pixels in image sequence in the time domain and the correlation between adjacent frames to find the correspondence between two frames. The algorithm proposed in this paper is based on the assumption of rigid motion, and the relative displacement between frames is calculated by numerical iteration. Compared with the optical flow method, the algorithm proposed by us is more convenient for the extraction of relative displacement between frames.

5. Results and Analysis

The junction region of absorption plates which is labeled with red box in Figure 5(c) is selected as the tracking template T. In the video image, there are about 537 pixels along the wide edge of the sound absorption plate with a width of 430 mm. Therefore, the dimension of one pixel is about 0.80 mm. Using the above displacement extraction algorithm, the response curve of vibration displacement is estimated as shown in Figure 8.

From the displacement curve shown in Figure 8, it can be seen that the vibration paces of displacements in the x and y directions are very similar. The waveform in the y direction contains more information and is much closer to the simulated response curve (Figure 4). The waveform in the

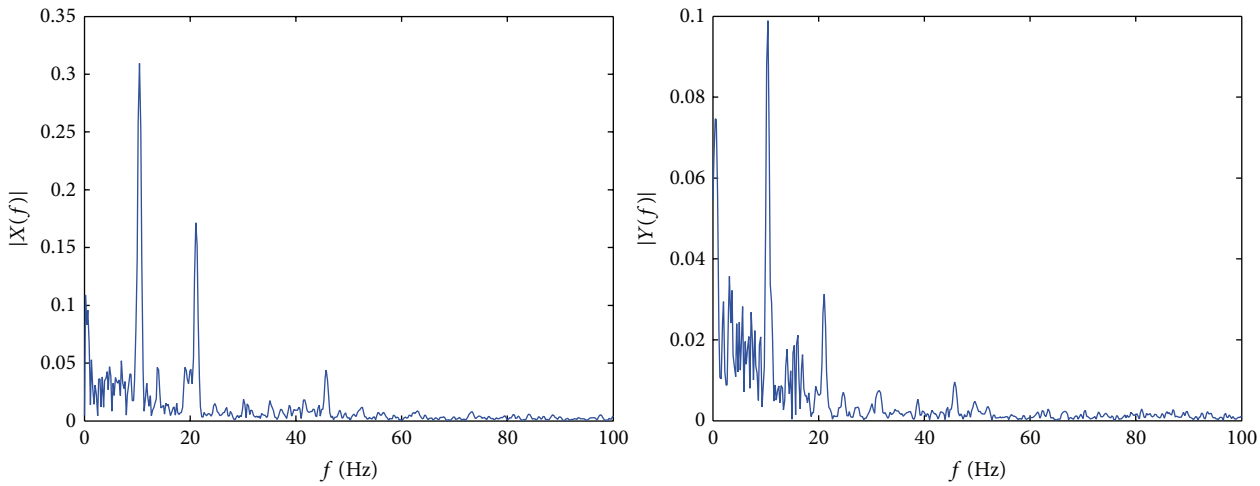

Figure 9: Spectrum of vibration response of sound barrier.

x direction is slightly cluttered but retains the peak clearly when the train reaches the sound barrier. The vibration in the y direction is more significant because the vibration of the sound barrier occurs mainly in the direction perpendicular to the plate surface.

It can be seen from the waveform in the y direction that the whole process of train passing is about 2 s. The vibration amplitude of the sound barrier is within ±2 mm. The arriving and leaving time of the train are labeled in Figure 8. The sound barrier vibration can be divided into the following phases: before the train arrives, the sound barrier vibrates slightly under environmental wind pressure; at 0.82 s, the train reaches the sound barrier, great positive and negative wind pressure is incited to intrude the sound barrier, and the sound barrier shifts facing the train to a maximum peak and quickly then shifts facing away from the train, resulting in head wave response; then the sound barrier vibrates under continuous excitation of the train-induced airflow; at 2.73 s, the train leaves the sound barrier, great positive and negative wind pressure opposite to that at 0.82 s is incited to intrude the sound barrier, and tail wave response with a lower peak value occurs; after the train leaves, the sound barrier vibration attenuates gradually and finally vibrates slightly under environmental wind pressure.

The Fourier spectrum of the vibration waveform is calculated as shown in Figure 9. It can be seen that the spectrums in the x and y directions are consistent. They both have significant peaks at 10.42 Hz, 21.07 Hz, and 45.77 Hz. The natural frequency of the viaduct is very low, about 2~4 Hz [16]. Therefore, these frequencies are the natural frequency of the sound barrier. The natural frequencies and the corresponding amplitudes of the sound barrier are shown in Table 1, which correspond exactly to the finite element simulation results. The natural frequency of the sound barrier is firstly obtained from in situ experiments via vibration video analysis.

It can be seen from the above analysis that the in situ detected vibration waveform has significant head wave and tail wave phenomenon similar to the simulation waveform, but relatively messy. This indicates that the sound barrier vibrates under more complex airflow rather than ideal steady flow field for simulation.

Table 1: Natural frequencies of sound barrier.

Order	Frequency/Hz	$\lvert Y(f)\rvert$
1	10.42	0.26
2	21.07	0.14
3	45.77	0.04

6. Conclusions

In conclusion, the influence of the impulsive wind pressure on the sound barrier during the whole process of train passing is revealed from the point of in situ experiment. The vibration of the sound barrier during the whole progress of train passing is recorded in situ by using high-speed cameras. Rigid displacement extraction algorithm based on the Taylor expansion is proposed to analyze the recorded video. The vibration response curve of the sound barrier is extracted successfully. Our method bridges the relationship between simulation and actual measurement and has important practical significance. Main conclusions of this study are as follows:

(1) The vibration response curve of the sound barrier obtained by high-speed imaging technology and the displacement extraction algorithm is consistent with the finite element simulation result. The in situ measurement verifies the head wave and tail wave phenomenon revealed in the simulation studies.

(2) The natural frequencies of the plug-in sound barrier are obtained from the spectrum analysis, which are 10.42 Hz, 21.07 Hz, and 45.77 Hz.

(3) High-speed imaging technology is an effective way to measure the sound barrier vibration. It can achieve noncontact and remote vibration measurement and has important practical value.

(4) For our displacement extraction algorithm based on Taylor expansion, displacement wave of rigid vibration can be extracted accurately without preinstallation of special markers on the tracking target. This algorithm needs fewer adjustable parameters, has high accuracy of subpixel, and is more automated.

Competing Interests

The authors declare that they have no competing interests.

Acknowledgments

This work was supported by Key University Science Research Project of Anhui Province (KJ2016A576) and Key University Science Research Project of Anhui Province (KJ2014A203).

References

[1] J. Lü, J. Zhang, J. Liao, W. Hu, and Y. Tu, "Response of noise barrier for existing railway bridges under impulsive pressure induced by high-speed train," *Journal of Southwest Jiaotong University*, vol. 44, no. 4, pp. 547–551, 2009.

[2] J. Hermanns, E. G. Giménez, and A. Alarcón, "Efficient computation of the pressures developed during high-speed train passing events," *Computers & Structures*, vol. 83, no. 10-11, pp. 793–803, 2005.

[3] C. Jiao, B. Gao, and G. Wang, "Vibration analysis of noise barrier structures subjected to train-induced impulsive wind pressure," *Journal of Southwest Jiaotong University*, vol. 429, no. 5, pp. 531–536, 2007.

[4] L. Zhao, L. Long, and Q. Cai, "Dynamic properties of noise barrier structure subjected to train-induced impulsive wind pressure," *Journal of Beijing University of Aeronautics and Astronautics*, vol. 35, no. 4, pp. 505–508, 2009.

[5] L. Long, L. Zhao, and L. D. Liu, "Research on the air turbulent pressure loaded on noise barrier caused by train," *Engineering Mechanics*, vol. 27, no. 3, pp. 246–250, 2010.

[6] M. Belloli, B. Pizzigoni, and F. ripamonti, "Fluid-structure interaction between trains and noise-reduction barriers: numerical and experimental analysis," *WIT Transactions on the Built Environment*, vol. 105, pp. 49–60, 2009.

[7] D. L. Wang, L. Zheng, and A. R. Chen, "Running cars induced wind loads on sound barrier of elevated roads," *Advanced Materials Research*, vol. 378-379, pp. 137–142, 2012.

[8] J. Zhao, J. Lin, J. Yao, and J. Ding, "Two-dimensional impact reconstruction method for rail defect inspection," *Mathematical Problems in Engineering*, vol. 2014, Article ID 236574, 9 pages, 2014.

[9] X. Lei, J. Guo, and C. Zhu, "Vision-based faint vibration extraction using singular value decomposition," *Mathematical Problems in Engineering*, vol. 2015, Article ID 306865, 14 pages, 2015.

[10] J. J. Lee and M. Shinozuka, "A vision-based system for remote sensing of bridge displacement," *NDT & E International*, vol. 39, no. 5, pp. 425–431, 2006.

[11] J. J. Lee and M. Shinozuka, "Real-time displacement measurement of a flexible bridge using digital image processing techniques," *Experimental Mechanics*, vol. 46, no. 1, pp. 105–114, 2006.

[12] H. Yang, T. Takaki, and I. Ishii, "Simultaneous dynamics-based visual inspection using modal parameter estimation," *Journal of Robotics and Mechatronics*, vol. 23, no. 1, pp. 180–195, 2011.

[13] S. W. Park, H. S. Park, J. H. Kim, and H. Adeli, "3D displacement measurement model for health monitoring of structures using a motion capture system," *Measurement*, vol. 59, pp. 352–362, 2015.

[14] H. Wang, A. Kläser, C. Schmid, and C.-L. Liu, "Dense trajectories and motion boundary descriptors for action recognition," *International Journal of Computer Vision*, vol. 103, no. 1, pp. 60–79, 2013.

[15] W. Chen and R. P. Mied, "Optical flow estimation for motion-compensated compression," *Image and Vision Computing*, vol. 31, no. 3, pp. 275–289, 2013.

[16] C.-Y. Kim, D.-S. Jung, N.-S. Kim, S.-D. Kwon, and M. Q. Feng, "Effect of vehicle weight on natural frequencies of bridges measured from traffic-induced vibration," *Earthquake Engineering and Engineering Vibration*, vol. 2, no. 1, pp. 109–115, 2003.